IJES *Iranian Journal of Earth Sciences*
Vol. 12, No. 4, 2020, 280-291.

Evaluation of land subsidence in Kashmar-Bardaskan plain, NE Iran

Hamid Saeidi[1], Gholamreza Lashkaripour*[1], Mohammad Ghafoori[1]

1. Department of Geology, Faculty of Science, Ferdowsi University of Mashhad, Iran

Received 18 September 2019; accepted 16 May 2020

Abstract

The development of agriculture and industry and the increase of population in countries with arid to semi-arid climates have led to more harvesting of groundwater resources and as a result land subsidence in different parts of the worlds. Decades of groundwater overexploitation in the Kashmar-Bardaskan plain in the north-east of Iran has resulted substantial land subsidence in this plain. The plain is considered as an arid to semi-arid zone and facing a negative water balance. The average annual precipitation in the plain is around 191 mm and the evaporation rate is 3956 mm. According to the unit hydrograph of the plain, the annual decline of water level is 1.12 m. In this study, the velocity of subsidence has been determined using Interferometric SAR technique (In-SAR) and radar images of Envisat ASAR and Sentinel-1 for a time period from 2003 to 2017. The results of an InSAR time series analysis indicated that an area of 1200 km^2 with different speeds of 5 to 26 cm/year in the satellite line of sight (LOS) is subsiding. The results showed that in addition to the decline of groundwater level, subsurface conditions such as sediments types (fine-grained layers) and their thickness also affect the occurrence and amount of land subsidence.

Keywords: *Aquifer compaction, Groundwater decline, Fine-grained material, Land subsidence*

1. Introduction

Land subsidence includes sinking or settlement of land surface due to diverse causes and generally occurs on a large scale. Usually, the terms refers to the vertical and downward movement of the land surface, although small-scale horizontal movements may be present (Poland 1984). The ongoing of land subsidence was documented using the relation between the declining groundwater levels and over-exploitation of the groundwater resources. Land subsidence is a global problem with many social and economic impacts, especially in developed urban, industrial and coastal areas (Abiding et al. 2015; Erkens et al. 2015). This phenomenon by changing the topography may increase flood vulnerability, reduce the quality of groundwater, create fissures and cracks, change groundwater levels, saltwater intrusion and reduce crop yields. Moreover, it may also cause damage to roads, subsurface infrastructure, and buildings (Hoffmann et al. 2003). The total damage caused by the land subsidence worldwide is estimated to be billions of dollars (Ward et al. 2011; Faunt et al. 2016). In recent decades, rapid population growth, agricultural expansion, and industrial development have led to an increase in the extraction of groundwater from aquifers. A long-term excessive groundwater withdrawal is considered to be a most important cause of land subsidence in many parts of the world, including 45 states of the United States (Galloway and Burbey 2011; Sneed and Brandt 2015). China has more than 45 cities and municipalities where disastrous land subsidence have occurred or are occurring (Guo et al. 2015; Peng et al. 2016; Chen et al. 2017; Liu et al. 2018).

*Corresponding author.
E-mail address (es): lashkaripour@um.ac.ir

There are many land subsidence areas have been noticed in the Japan (Yamamoto 1995; Furuno et al. 2015). Similarly, countless subsidence have occurred in Chile, Indonesia, Thailand, Italy and Turkey (Üstün et al. 2015), Greece, Mexico (Calderhead et al. 2011), France and Spain, etc. (Ruiz-Constán et al. 2016). There are a variety of methods available for monitoring the land subsidence. The conventional techniques include repeat optical leveling and the global positioning system (GPS) surveys, ground reconnaissance, photo-geological analysis, groundwater monitoring, and tape-extensometers. Also, the advanced techniques include the processing and interpretation of differential interferograms of repeat-pass, satellite-based synthetic aperture radar data (InSAR; Fergason et al. 2015).

In Iran, as in other parts of the world, excessive water extraction has caused land subsidence throughout the country. This phenomenon is reported to have affected many major cities and plains across Iran, which include different plains like Tehran (Alipour et al. 2008; Sadeghi et al. 2013; Mahmoudpour et al. 2016), Mashhad (Motagh et al. 2007; Dehghani et al. 2009a; lashkaripour et al. 2014), Neyshabour (Dehghani et al. 2009b; Lashkaripour and Ghafoori 2009), Rafsanjan (Mousavi et al. 2001; Dehghani et al. 2014; Motagh et al. 2017), Mahyar, Isfahan Province (Salehi et al. 2012; Davoodijam et al. 2015), Zarand, Kerman Province (Motagh et al. 2008), Hashtgerd, west of Tehran (Dehghani et al. 2008) and Saveh sub-basin, Markazi Province (Jafari et al. 2016).

Kashmar-Bardaskan plain like other agricultural regions of the country has been adversely affected by land subsidence due to overexploitation of the groundwater. The resident population in the plain has grown rapidly by 36 percent, i.e. from 217,417 to 295,996 during 1986 to 2016 (Statistical Center of Iran, 2016). Most of residents

in the region are farmers. Earth fissures and cracks caused by land subsidence in the south-west of Kashmar city, were studied in an earlier study by Lashkaripour et al. (2009). Anderssohn et al. (2008) analyzed Envisat ASAR images with InSAR technique during the period 2003-2006 and determined land subsidence for a part of Kashmar Bardaskan Plain.

The main objective of present study is to define the entire subsidence area and spatial and temporal changes in land subsidence in the Kashmar-Bardaskan plain, using Envisat ASAR and Sentinel-1 images. The effective factors like rate of aquifer recharge and discharge and groundwater fluctuation by pumping from wells are also to be determined.

.

2. Study area

2.1. Location and physiography

Kashmar-Bardaskan plain is located in Khorasan Razavi province northeast of Iran. It is around100 km long valley having a width of 10 km toward east and more than 20 km toward west and covering an area of 1800 km^2. Its drainage basin encompasses more than 1880 km^2. Maximum elevation in the northern mountain ranges is 2715 m and minimum elevation of about 710 m of sea level is located in the floor of the valley. Doruneh active fault is the most important morph tectonic complication of the study area. The permanent rivers Sang-e-nasuh (Kashmar), Sheshtraz and the seasonal Dahan Ghaleh are the most important surface currents in the study area. They flow southward into the valley from northern mountains and deposit large alluvial fans throughout the northern parts of the plain (Fig 1).

2.2. Climate

The climate of the study area has been categorized based on De Martonne's modified classification as mild arid to hyper arid. Based on the collective data sets from Kashmar Synoptic Station during 1985-2014, the average annual precipitation is 191 mm and temperature is in the range of -5.3 to 34.4 °C. Based on the data of the Doruneh station, the average annual evaporation in the Kashmar-Bardaskan plain is 3956mm.

2.3. Geology

The study area is located in the north of the central Iranian micro-continent. Doruneh fault forms the northern boundary between north mountain ranges and depression of Kashmar-Bardaskan. It has east-west trending with left lateral strike-slip movement (Wellman 1966; Stocklin and Nabavi 1973; Fattahi et al. 2006; Farbod et al. 2016).

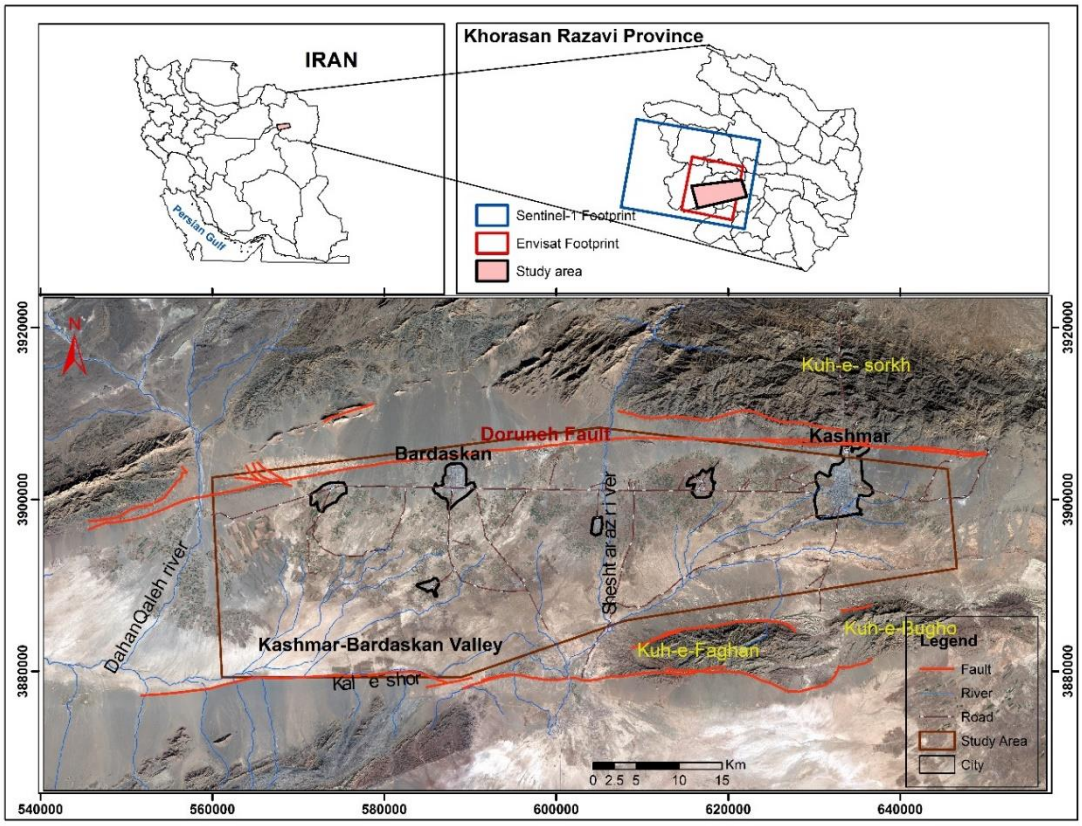

Fig 1. Geographical location of the study area in Sentinel-2 image

In the Quaternary, the tectonic activity of the Doruneh fault with large extent climatic variation had led to the deposition of widespread alluvial fans that repeated the cycle of tectonic movements and climatic impulses,

which caused erosion of the alluvial fans and deposition on Kashmar-Bardaskan depression (Giessner et al. 1984). The southern boundary of the Quaternary sediments is the Kal-e-Shour fault, which caused the formation of lagoon and playa in the southern part of the plain. Rock outcrops in the northern mountain ranges are divided into four major units: 1). Magmatic Arc contains volcano-plutonic rocks, 2). Taknar Inlier consists of Paleozoic and Mesozoic sedimentary and metamorphic rocks, meta rhyolite and rhyodacite and granite-granodiorite (Muller and Walter 1983), 3). Ophiolitic complex and 4). Eocene Flysch type deposits consist of more than 6000 m pyroclastic, volcanic and flysch sedimentary rocks. Southern mountains consist of a series of Paleozoic, Mesozoic and Cenozoic sedimentary rocks. Unconsolidated to poorly consolidated Quaternary basin-fill deposits fill Kashmar-Bardaskan Valley, included old and young terraces, loose recent alluvium, and gravel and gravelly fan and the deposits of the alluvial fan , floodplain (clay flats), wind (sand sheets and sand dunes), salt flat and playa lake (Fig 2).

2.4. Hydrology

Improper water management in the study area has a negative impact, such as the destruction of aquifers, groundwater fluctuations, land subsidence, water quality degradation, and negative economic and social impacts. An accurate assessment of groundwater balance is important for proper water resources management. Table 1 shows the ground water balance for Kashmar-Bardaskan aquifer from 2010-2011. Based on the plain water balance, there is -76 mcm overexploitation per year from the aquifer. This eliminates the equilibrium in the aquifer and the negative trend of volume changes.

3. Groundwater development

Pumping from wells is the largest water withdrawal from the Kashmar-Bardaskan aquifer, and is the most important factor controlling short-term and long-term groundwater levels fluctuations. The 84 percent water is used for irrigation, 9 percent for municipal, and the rest in the industries and other purposes. The location of exploitation wells and discharge rates from 1976 to 2014 in the plain is shown in figure 3. Since 1976, the general trend of groundwater withdrawal from the aquifer has been increased (Fig 4).

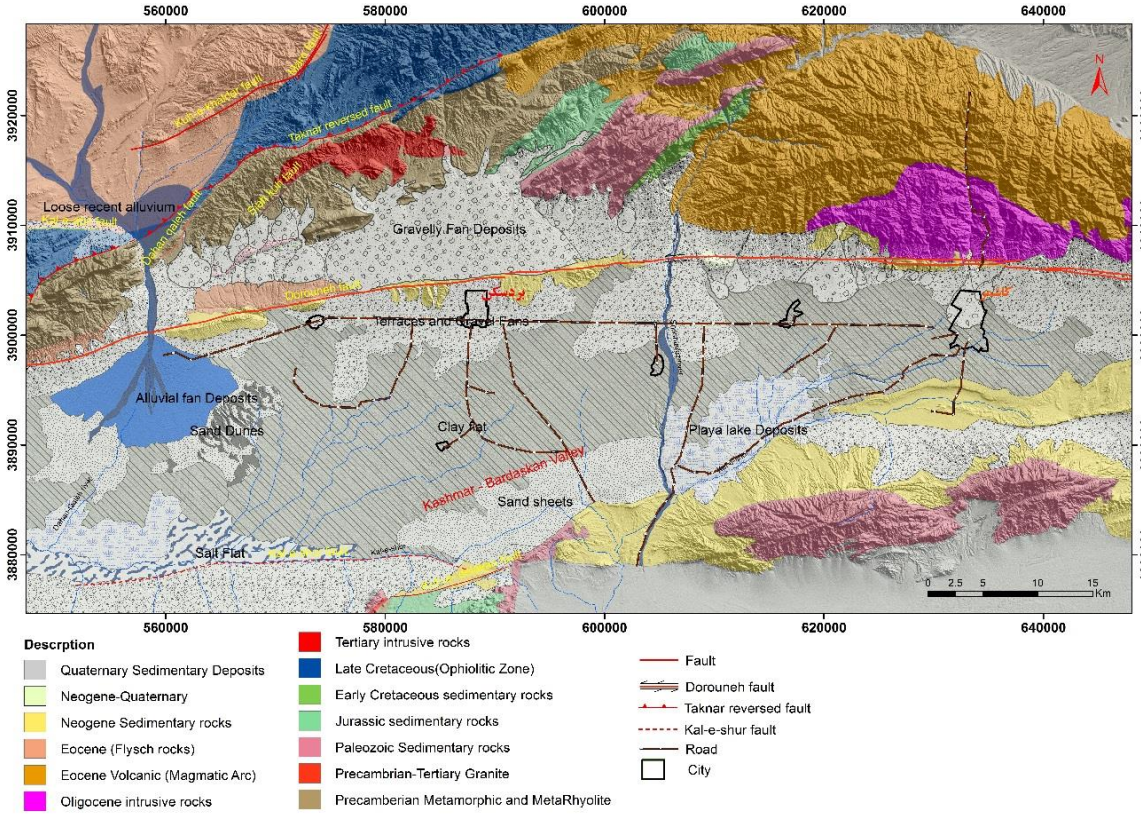

Fig 2. Geological map of the study area (modified from Geological survey of Iran, Taheri and Shamanian.1998; Shahrabi et al. 2006)

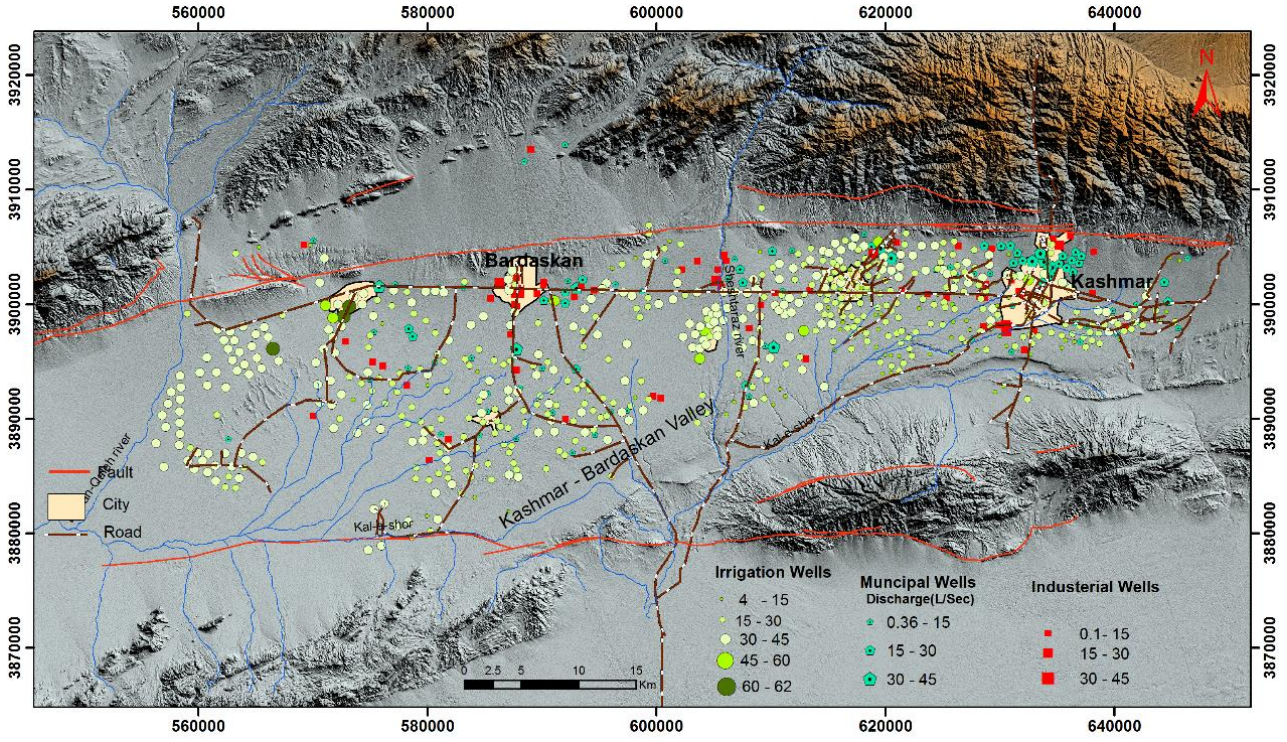

Fig 3. Exploitation well locations, types and discharge rates in Kashmar-Bardaskan plain (1976-2014)

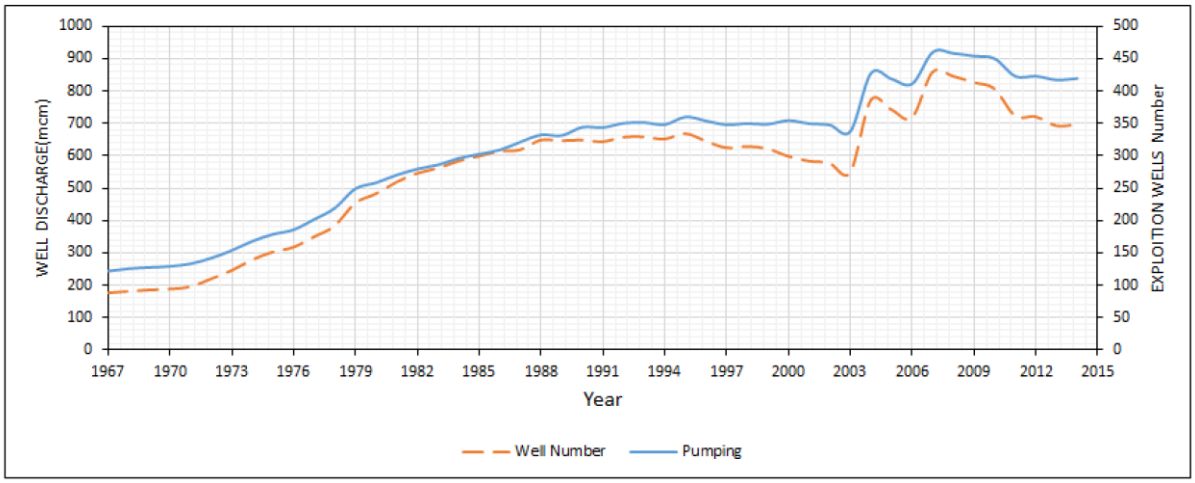

Fig 4. Relation between exploitation wells and cumulative discharge for the period between 1967 to 2014

However, the number of wells is dramatically increased after 2003 and presently the amount of discharge from these wells is around 100 million cubic meters per year. Long-term changes in groundwater level due to water withdrawal by exploitation wells in Kashmar-Bardaskan plain have been investigated. In this study, the data from 26 piezometric wells from September 1998 to March 2017 were collected to produce unit hydrograph and groundwater-surface map changes. The unit hydrograph of the plain has a descending trend and is an approximately straight line (Fig 5). The reason for such behavior is the uninterrupted and continuous using of groundwater from wells. The average annual decline of groundwater is around 1.12 m, which indicates a reduction in the reservoir of groundwater and a negative plain water balance.

The groundwater level decline in the plain is increasing with time (Fig 6). The maximum groundwater decline occurred in the northern part of the aquifer was around -88.41 m. That region comprises thick layers of coarse grain fluvial terraces and alluvial fan sediments with high permeability and good water quality.

Table 1. Conceptual groundwater balance during 2010-2011 for the Kashmar-Bardaskan aquifer (Modified from Khorasan Razavi Regional Water Authority, 2016)

		Million cubic meter/Year
RECHARGE	Bedrock inflow from surrounding mountains	87.64
	Seepage from rivers and flood water	31.23
	Infiltration of precipitation falling on unconsolidated basin fill	55.12
	Infiltration from irrigation water from surface water and ground water sources	96.56
	Infiltration from wastewater effluent and industrial	26.22
	Subsurface inflow	4.87
	Total recharge	301
DISCHARGE	Wells, springs, qantas, surface water	375.38
	Evapotranspiration from aquifer	1.63
	Subsurface outflow	0.63
	Total discharge	377
Budget	Discharge-Recharge	-76

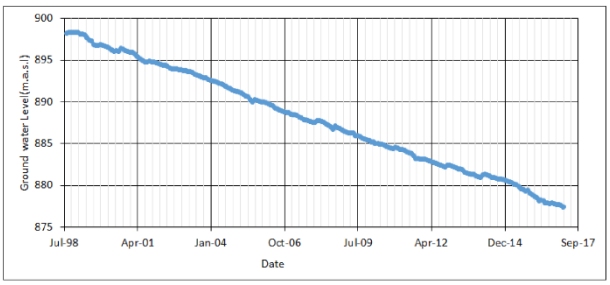

Fig 5. Unit hydrograph for the period 1998 to 2017 in Kashmar-Bardaskan plain

Therefore, most of the industrial and municipal wells with high discharge have been excavated in this region (Fig 3). The fine-grained soil of the floodplain lies in the middle part of the plain (Clay flat), which is fertile and used for agricultural purposes. High water extraction by wells for agriculture purposes has led to the decline of -10 to -40 m in groundwater level from 1998 to 2017. The lowest groundwater level of 2 m decline is noticed from the southern parts that may be due to very bad water quality and lack of residents in the region.

4. Aquifer characteristics

The unconfined aquifer of Kashmar-Bardaskan plain is composed of Quaternary sediments. Quaternary sediments consist of coarse grain fluvial terraces and alluvial fan sediments, which composed of thick layers, poorly to well sorted of clay, silt, sand, gravel and boulders. Sediments with higher permeability are located throughout the northern part of the aquifer. These sediments result from the erosion of igneous rocks in the highlands of the northern aquifer. Fine-grained sediments in the center of the aquifer compose low-permeability silt, and clay with fine sands and salt flats associated with gypsum deposits in the southern part of the aquifer result from the erosion of Neocene and gypsiferous red beds formations that placed in southern mountains chain. Soil texture, distribution and thickness of sediments on bedrock effect on aquifer compressibility and the land subsidence rates.

4.1. Thickness of sediments

Using the information of existing piezometer wells and geoelectical studies, the bedrock topography and thickness of sediments were determined (Fig 7). The maximum thickness of sediment or depth of bedrock was determined in the southern part of Doruneh fault. The results indicate that the sediment thicknesses vary from 50 to > 400 m and the depth of the bedrock reduces from the north to the south. The slope of the bedrock increases from east to west.

4.2. Aquifer sediments texture

Distribution and composition of aquifer sediments are determined by using existing data for the plain. In order to determine the percentage of fine and coarse-grained sediments and thickness of compressible sediments (clay and silt), the borehole log of 21 piezometric wells and 144 exploitation wells were used. The depth of drilled wells range from 50 to 280 m in this plain. By determining the percentage of fine-grained deposits for all wells and interpolation, the percentage and lateral extension of the soil texture were obtained for Kashmar-Bardaskin plain (Fig 8). As shown in figure 8, toward the center and south of the plain, the percentage of fine-grained sediments increased. According to geoelectric studies and the borehole log of exploitation wells, the bedrock consists of sandstone, claystone, and marl with gypsum.

5. Land subsidence

The Interferometric Synthetic Aperture Radar (InSAR) technique was used to determine the temporal evolution of the land subsidence in this plain. For this purpose, 40 Envisat ASAR single look complex (SLC) images in descending mode from track 435 from 20 March 2003 to 9 September 2010 were collected to generate differential Interferograms. Because the Envisat images do not cover the entire area of subsidence, 26 sentinel- 1A_IW_SLC in Tops mode in descending Track with a time period from Sep 2014 to Sep 2017 were obtained. The small baseline subset (SBAS) algorithm is used for InSAR time-series analysis (Berardino et al. 2002). Cumulative of the subsidence phase was obtained by the least squares method. Finally, the mean line of sight (LOS) displacement velocity map was obtained from InSAR time series analysis.

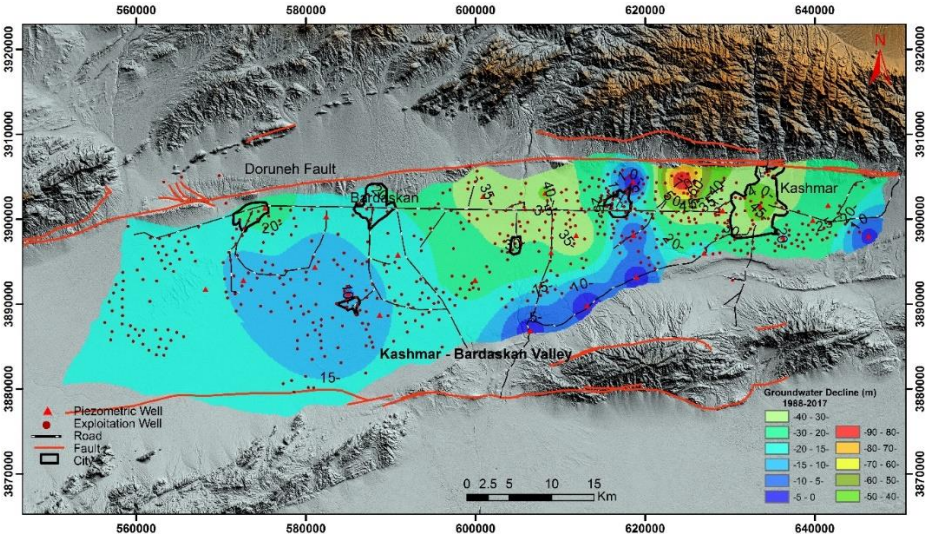

Fig 6. Map of groundwater decline with exploitation and piezometric wells in Kashmar-Bardaskan plain from the period 1998 to 2017.

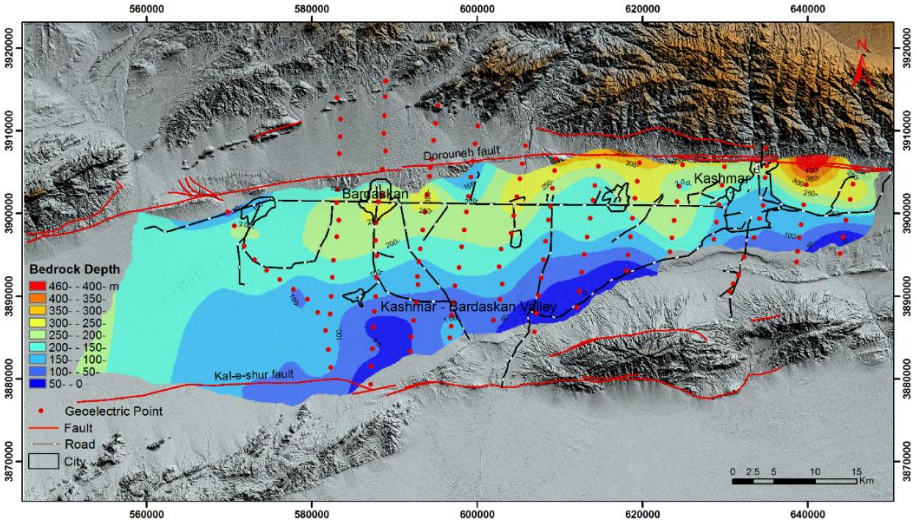

Fig 7. Map of bedrock depth or thickness of sediments in Kashmar-Bardaskan plain

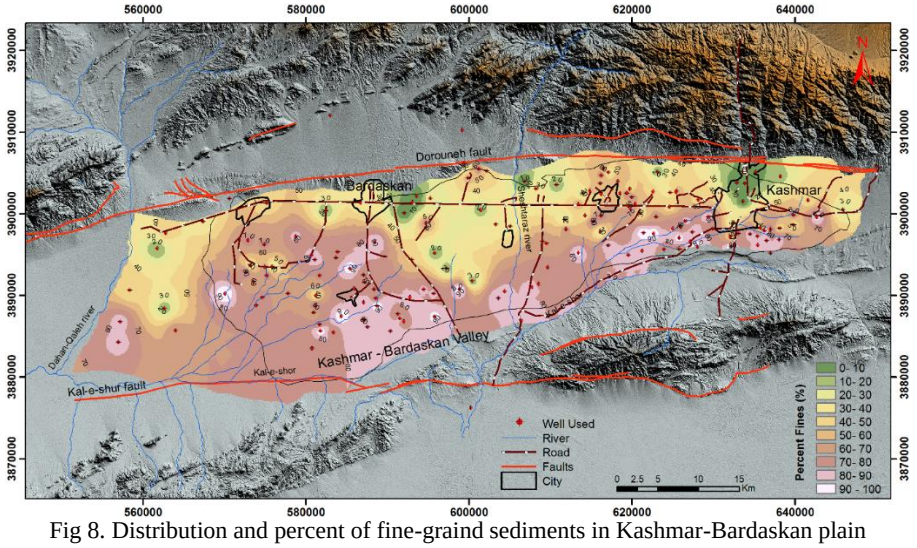

Fig 8. Distribution and percent of fine-graind sediments in Kashmar-Bardaskan plain

Figure 9 shows the annual mean velocity of subsidence along the satellite LOS, which was obtained from processing Envisat ASAR (Fig 9a) and Sentinel-1 (Fig 9b) images in the plain. According to figure 9, the subsidence signal is very clear and stretches in the direction of the plain. The pattern of the subsidence area is similar in two sensors. The area of 1,200 km^2 is subjected to subsidence that exceeded 5cm/year. As shown in figure 9a, the subsidence area in the western part of the plain is more widespread than the other parts. The maximum annual displacement rate derived from SBAS processing of Envisat SAR data is 26 cm. During 2014-2017, it seems that the land subsidence extended more toward the middle and eastern parts of the plain (Fig 9b). This point is clearly noticeable in the subsidence bowl at southwest Kashmar city. The maximum annual displacement rate along the line of sight is 21 cm. Due to relatively steep Sentinel-1 incidence angle, the maximum vertical annual subsidence rate is about 29 cm per year. In figure 10, the results of land subsidence in the Kashmar-Bardaskan plain are shown.

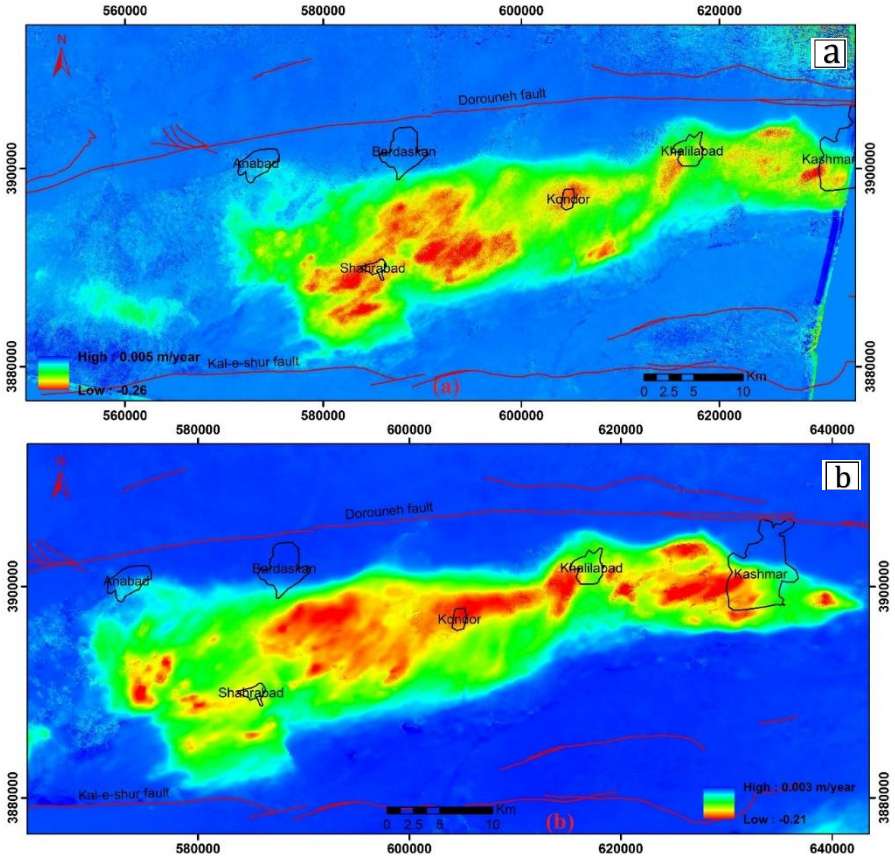

Fig 9. Mean LOS velocity displacement rate of subsidence derived from (a) Envisat descending (b) Sentinel-1 descending images

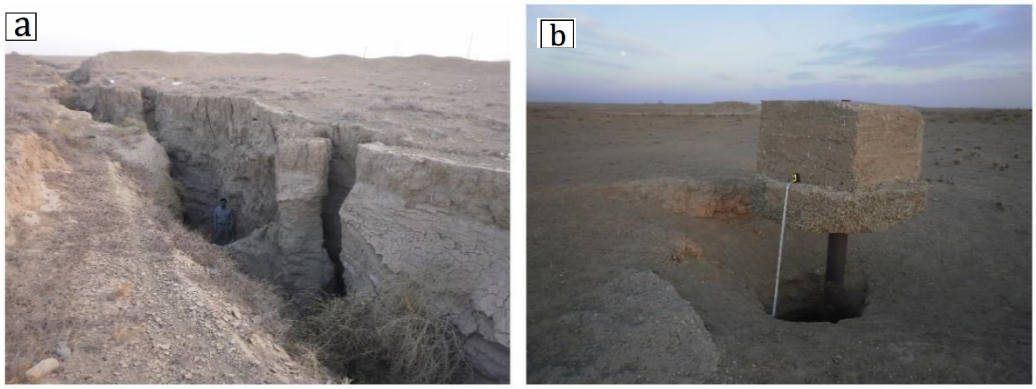

Fig 10. The evidence of land subsidence in Kashmar-Bardaskan Plain (a) Surface fissures (b) Extruded well casing

6. Discussion

The results of this study showed that two important factors influence the land subsidence of Kashmar-Bardaskan plain. The first is the condition and type of subsurface sediments and the second is the groundwater level decline. In order to investigate the effect of sediments thickness and soil texture (fine or coarse grained) on the extent and velocity rate of subsidence in this plain, surface clay-flat area and depth to bedrock or thickness of sediments are superimposed on the land subsidence map (Fig11). The result shows that land subsidence occurs in surface clay-flat area. The maximum subsidence bowls are located in the western (points A, B, C and D) and eastern (point E) parts of the plain. The thickness and proportion of fine-grained (silt and clay) or compressible sediments is >100 m and > 60 %,respectively.Groundwater depletion from exploitation wells is the main water supply source in the study area. To evaluate the influence of the pumping wells on land subsidence, the map of subsidence rate and decline of groundwater level was compared (Fig 12). Figure 12a presents the groundwater level changes within Kashmar-Bardaskan aquifer during 1998-2010 with subsidence rate derived from Envisat ASAR sensor. According to this map, the groundwater decline in the clay flat ranged from -10 to -25 m. the land subsidence bowels comprising points A, B, C and D in the western part and point E largely overlapped with groundwater decline bowels.

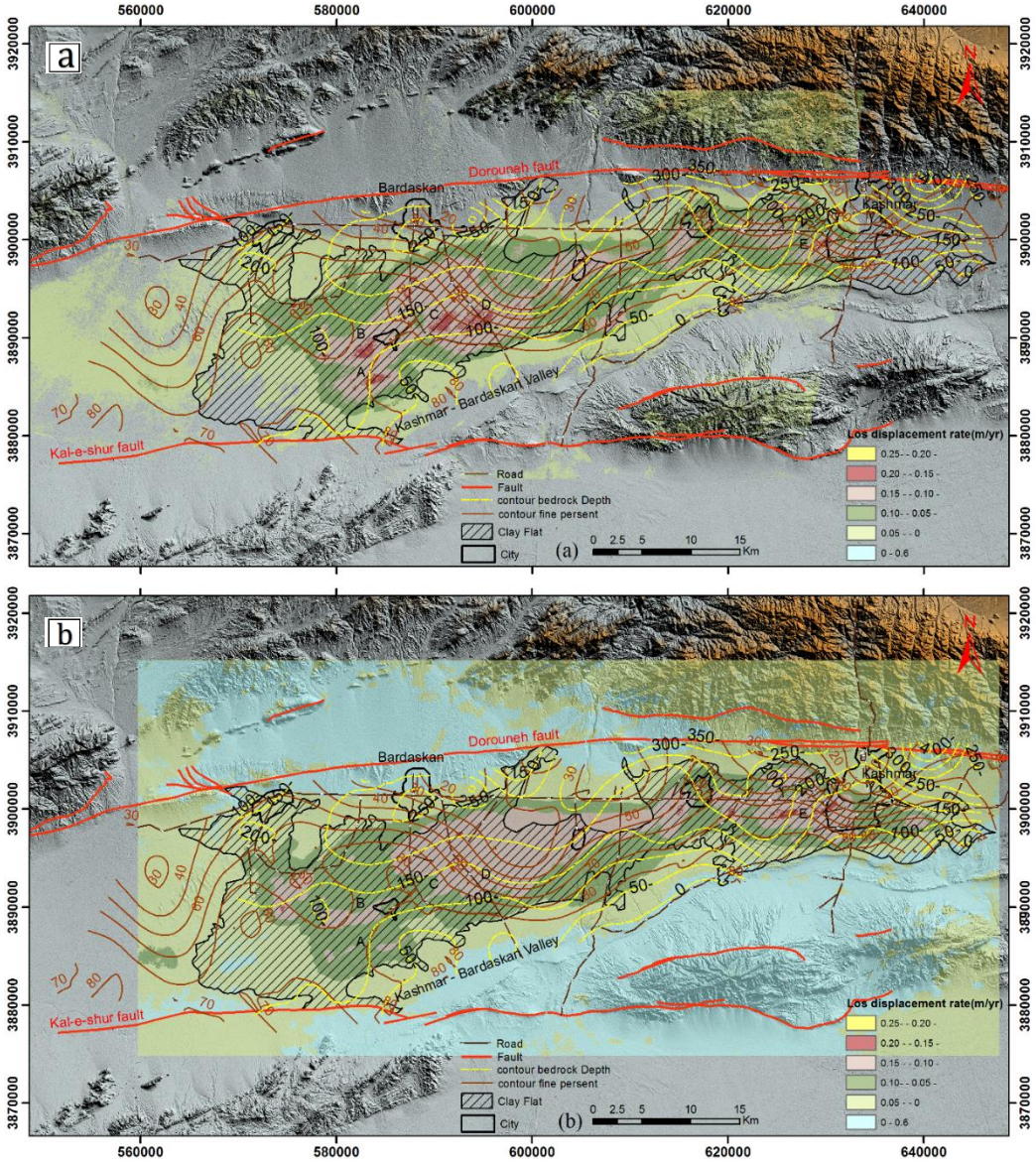

Fig 11. The relationships between land subsidence and aquifer sediments (a) Envisat Images (b) Sentinel-1 images

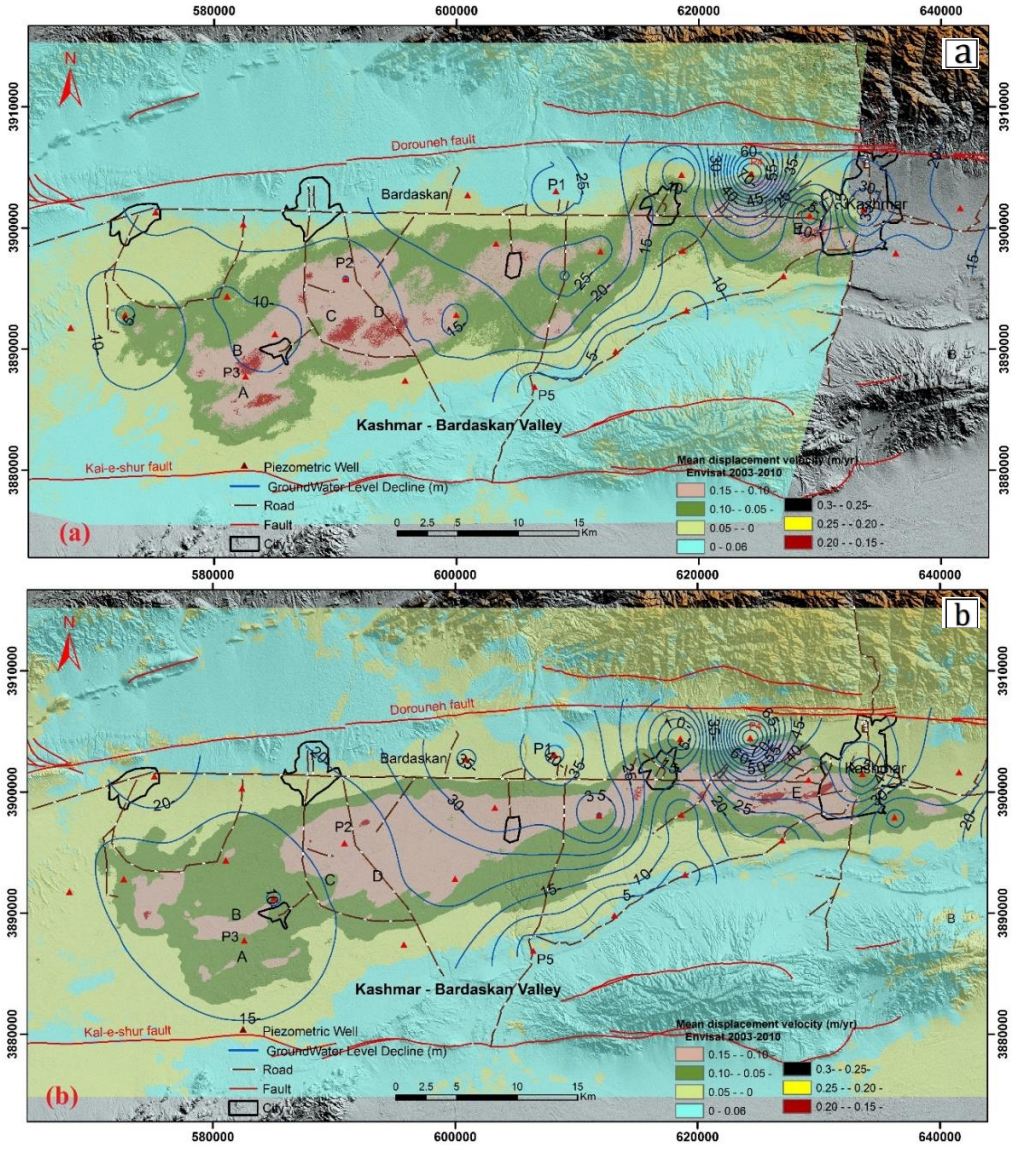

Fig 12. The relation between land subsidence rate and groundwater level changes (a) Envisat images (b) Sentinel-1 images

Figure 12b presents the groundwater-level changes for the period of 1998-2017 with subsidence rate from Sentinel-1 images. As shown in this figure, rate of groundwater-level decline in the plain is increasing with time from 1998 to 2017.

It can be seen that the land subsidence decreased and the bowls disappeared in the western parts (points A, B, C, and D). In contrast, the amount of land subsidence in the central and eastern parts of the plain has been increased (point E), which shows that the decline in groundwater level and the land subsidence rate are closely correlated. Figure 13 illustrates the time series of the groundwater level changes versus amount of land subsidence measured by In-SAR, which corresponds to Envisat and Sentinel images at five piezometers location from the time period from 2003 to 2010 and 2014 to 2017. P1 is located in coarse-grained alluvial fan sediments in the northern part of the plain. The percentage of fine-grained silt and clay sediments increases toward the south especially at P5. In all piezometric wells, except for the P5, the groundwater level is clearly declining with a steep slope without significant seasonal fluctuations. P5 is located in the southern part of the plain outside subsidence area and at the intersection of the seasonal rivers, which is sometimes fed. In this location groundwater quality is bad and there is almost no water depletion. The amount of annual subsidence is closely correlated with groundwater level variations in the piezometric wells P2, P3 and P4. The annual subsidence rate for 1 m of decline groundwater table for these piezometric wells is 12.8, 17.3 and 3.7 cm for the time period of 2003 to 2010 and 25, 17 and 8 cm from 2014 to

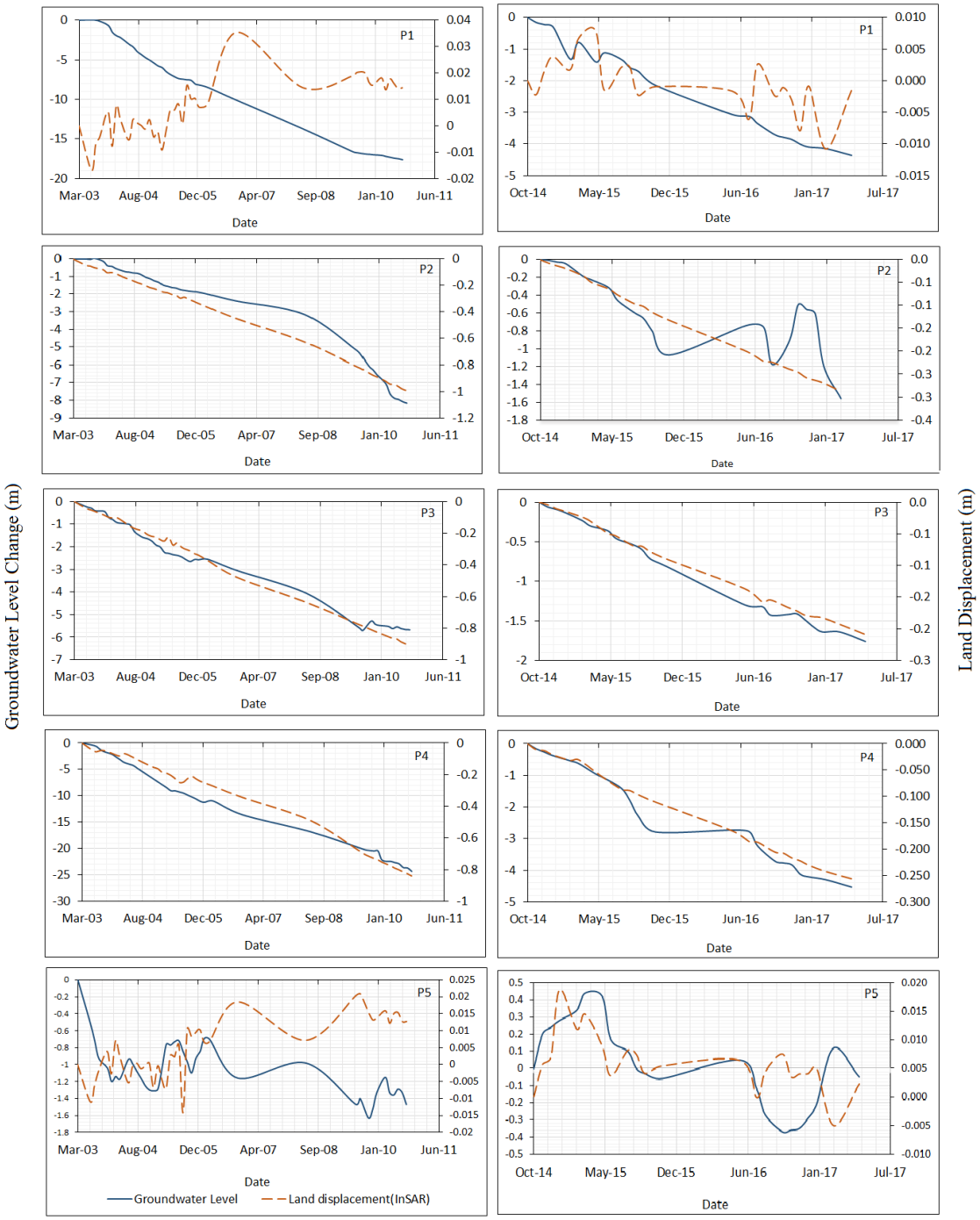

Fig 13. Relation between the amount of subsidence and piezometric groundwater level changes

2017, respectively. This means that land subsidence decrease in the western part of the plain from 2014-2017 and increase in the central and eastern parts. The solution to reduce land subsidence in this plain is to better manage the extraction of water resources by cultivating plants that need less water.

7. Conclusions

Using the In-SAR technique and processing Envisat and Sentinel-1 radar images, land subsidence has been determined from 2003-2010 and 2014-2017 for Kashmar-Bardaskan plain, Iran. Time series analysis shows that the region of subsidence is a stretched area of 1200 km^2 with an east-west orientation in accordance with the geomorphology of the plain. The subsidence rate decreased during the time period studied from the west of the plain, but it has increased in the center and east of the plain. The mean velocity displacement rate in the satellite line of sight (LOS) is 5-26 cm/year. Geophysical studies indicate that the bedrock is not uniform. The slope of the

plain is from east to west of the plain. The depth of the bedrock increase from the southern mountain to the Quaternary Doruneh fault in the northern plain. Its maximum depth is around the Doruneh fault covered by coarse-grained alluvial fan sediments.

According to the soil texture map, the maximum depth of the fine-grained silt and clay sediments is in the middle and west parts of the plain. The continuous and excessive water withdrawal by the pump caused a 1.12 m annual decline in groundwater level, which is the main cause of subsidence in the plain. Comparison of the results shows that there is a good correlation between the subsidence area with depth and distribution of fine-grained sediments and the amount of groundwater decline in the plain.

Acknowledgements

The authors would like to thank the Regional Water Company of Khorasan e Razavi for providing the necessary data. We would also like to thank for Envisat SAR data were provided by the European Space Agency under research proposal ID 32232 and Sentinel-1 data provided by ESA/Copernicus. Part of the data processing is done at HPC (High-Performance Computing) center of Ferdowsi University of Mashhad and we thank them for their help.

References

Abidin HZ, Andreas H, Gumilar I, Sidiq TP, Gamal M (2015) Environmental impacts of land subsidence in urban areas of Indonesia, In *FIG Working Week* 1-12.

Alipour S, Motgah M, Sharifi MA, Walter TR (2008) InSAR time series investigation of land subsidence due to groundwater overexploitation in Tehran, Iran, *In use of Remote Sensing Techniques for Monitoring Volcanoes and Seismogenic Areas, IEEE:* 1-5.

Anderssohn J, Wetzel HU, Walter TR, Motagh M, Djamour Y, Kaufmann H (2008) Land subsidence pattern controlled by old alpine basement faults in the Kashmar Valley, northeast Iran: results from InSAR and levelling, *Geophysical Journal International* 174(1): 287-94.

Berardino P, Fornaro G, Lanari R, Sansosti E (2002) A new algorithm for surface deformation monitoring based on small baseline differential SAR interferograms, *IEEE Transactions on Geoscience and Remote Sensing* 40(11): 2375-83.

Calderhead AI, Therrien R, Rivera A, Martel R, Garfias J (2011) Simulating pumping-induced regional land subsidence with the use of InSAR and field data in the Toluca Valley, Mexico, *Advances in Water Resources 34*(1): 83-97.

Chen B, Gong H, Li X, Lei K, Zhu L, Gao M, Zhou C (2017) Characterization and causes of land subsidence in Beijing, China, *International journal of remote sensing* 38(3): 808-26.

Davoodijam M, Motagh M, Momeni M (2015) Land Subsidence in Mahyar Plain, Central Iran, Investigated Using Envisat SAR Data. - In: Kutterer, H., Seitz, F., Alkhatib, H., Schmidt, M. (Eds.), *the 1st International Workshop on the Quality of Geodetic Observation and Monitoring Systems (QuGOMS'11)*, (International Association of Geodesy Symposia; 140), Cham: *Springer International Publishing*: 127-130.

Dehghani M, Zoej MV, Bolourchi MJ, Shemshaki A, Saatchi S (2008) Monitoring of Hashtgerd land subsidence induced by overexploitation of groundwater using SAR interferometry, *Geosciences* 17(1): 223-32.

Dehghani M, Zoej MJ, Saatchi S, Biggs J, Parsons B, Wright T (2009a) Radar interferometry time series analysis of Mashhad subsidence, *Journal of the Indian Society of Remote Sensing* 37(1): 147-56.

Dehghani M, Valadan Zoej MJ, Entezam I, Mansourian A, Saatchi S (2009b) InSAR monitoring of progressive land subsidence in Neyshabour, northeast Iran, *Geophysical Journal International* 178(1): 47-56.

Dehghani M, Rastegarfar M, Ashrafi RA, Ghazipour N, Khorramrooz HR (2014) Interferometric SAR and geospatial techniques used for subsidence study in the Rafsanjan plain, *American Journal of Environmental Engineering* 4(2): 32-40.

Erkens G, Sutanudjaja EH (2015) Towards a global land subsidence map, *Proceedings of the International Association of Hydrological Sciences* 372: 83-87.

Farbod Y, Shabanian E, Bellier O, Abbassi MR, Braucher R, Benedetti L, Bourles D, Hessami K (2016) Spatial variations in late Quaternary slip rates along the Doruneh Fault System (Central Iran), *Tectonics* 35(2):386-406.

Fattahi M, Walker R, Hollingsworth J, Bahroudi A, Nazari H, Talebian M, Armitage S, Stokes S (2006) Holocene slip-rate on the Sabzevar thrust fault, NE Iran, determined using optically stimulated luminescence (OSL), *Earth and Planetary Science Letters* 245(3-4):673-84.

Fergason KC, Rucker ML, Panda BB (2015) Methods for monitoring land subsidence and earth fissures in the Western USA, *Proceedings of the International Association of Hydrological Sciences* 372: 361-6.

Faunt CC, Sneed M, Traum J, Brandt JT (2016) Water availability and land subsidence in the Central Valley, California, USA, *Hydrogeology Journal* 24(3): 675-684.

Furuno K, Kagawa A, Kazaoka O, Kusuda T, Nirei H (2015) Groundwater management based on monitoring of land subsidence and groundwater levels in the Kanto Groundwater Basin, Central Japan, *Proceedings of the International Association of Hydrological Sciences* 372:53-7.

Galloway DL, Burbey TJ (2011) Regional land subsidence accompanying groundwater extraction, *Hydrogeology Journal* 19(8): 1459-86.

Giessner K, Hagedorn H, Sarvati MR (1984) Geomorphological studies in the Kashmar region (NE Iran), *Neues Jahrbuch für Geologie und Paläontologie, Abhandlungen Band 168 Heft* 2-3: 545-57.

Guo H, Zhang Z, Cheng G, Li W, Li T, Jiao JJ (2015) Groundwater-derived land subsidence in the North China Plain, *Environmental earth sciences* 74(2): 1415-27.

Hoffmann J, Leake SA, Galloway DL, Wilson AM (2003) MODFLOW-2000 ground-water model--User guide to the subsidence and aquifer-system compaction (SUB) package, *Geological Survey Washington DC*.

Jafari F, Javadi S, Golmohammadi G, Karimi N, Mohammadi K (2016) Numerical simulation of groundwater flow and aquifer-system compaction using simulation and InSAR technique: Saveh basin, Iran, *Environmental Earth Sciences* 75(9): 833.

Lashkaripour GR, Ghafoori M (2009) Land subsidence due to groundwater level decline in Neyshabur plain, Ne Iran, *In the 1st Regional Conference on Geo-Disaster Mitigation and Waste Management*.

Lashkaripour GR, Ghafoori, M, Rostamibarani H (2009) investigating the causes of fissures formation and subsidence in the west of Kashmar plain, *Geological Studies* 1(1): 95-111. (in Persian)

Lashkaripour GR, Ghafoori M, Moussavi Maddah SM (2014) An investigation on the mechanism of land subsidence in the northwest of mashhad city, NE Iran, *Journal of Biodiversity and Environmental Sciences* 5(3): 321-327.

Liu Y, Zhao C, Zhang Q, Yang C, Zhang J (2018) Land Subsidence in Taiyuan, China, Monitored by InSAR Technique With Multisensor SAR Datasets From 1992 to 2015, *IEEE Journal of Selected Topics in Applied Earth Observations and Remote Sensing* 11(5):1509-1519.

Mahmoudpour M, Khamehchiyan M, Nikudel MR, Ghassemi MR (2016) Numerical simulation and prediction of regional land subsidence caused by groundwater exploitation in the southwest plain of Tehran, Iran, *Engineering Geology* 201:6-28.

Mousavi SM, Shamsai A, Naggar MH, Khamehchian M (2001) A GPS-based monitoring program of land subsidence due to groundwater withdrawal in Iran, *Canadian journal of civil engineering* 28(3): 452-64.

Motagh M, Djamour Y, Walter TR, Wetzel HU, Zschau J, Arabi S (2007) Land subsidence in Mashhad Valley, northeast Iran: results from InSAR, levelling and GPS, *Geophysical Journal International* 168(2): 518-26.

Motagh M, Walter TR, Sharifi MA, Fielding E, Schenk A, Anderssohn J, Zschau J (2008) Land subsidence in Iran caused by widespread water reservoir overexploitation, *Geophysical Research Letters* 35(16): L16403.

Motagh M, Shamshiri R, Haghighi MH, Wetzel HU, Akbari B, Nahavandchi H, Roessner S, Arabi S (2017) Quantifying groundwater exploitation induced subsidence in the Rafsanjan plain, southeastern Iran, using InSAR time-series and in situ measurements, *Engineering Geology* 218: 134-51.

Muller R, Walter R (1983) Geology of the Precambrian-Paleozoic Taknar inlier, northwest of Kashmar, Khorasan province, northeast Iran, *Geological Survey of Iran, Tehran, Report* 50: 252.

Peng JB, Sun XH, Wang W, Sun GC (2016) Characteristics of land subsidence, earth fissures and related disaster chain effects with respect to urban hazards in Xi'an, China, *Environmental Earth Sciences* 75(16): 1190.

Poland JF (1984) Guidebook to studies of land subsidence due to ground-water withdrawal, Paris: *Unesco*.

Ruiz-Constán A, Ruiz-Armenteros AM, Lamas-Fernández F, Martos-Rosillo S, Delgado JM, Bekaert DP, Sousa JJ, Gil AJ, Cuenca MC, Hanssen RF, Galindo-Zaldívar J. Multi-temporal (2016) InSAR evidence of ground subsidence induced by groundwater withdrawal: the Montellano aquifer (SW Spain), *Environmental Earth Sciences* 75(3): 242.

Sadeghi Z, Zoej MJ, Dehghani M (2013) An improved persistent scatterer interferometry for subsidence monitoring in the Tehran Basin. *IEEE Journal of Selected Topics in Applied Earth Observations and Remote Sensing* 6(3): 1571-7.

Salehi R, Ghafoori M, Lashkaripour GR, Dehghani M (2012) Investigation of land subsidence in southern Mahyar Plain in Esfahan province, Iran. *International Journal of Emerging Technology and Advanced Engineering* 2(9): 389-394.

Shahrabi M, Hosseini M, Shabani K (2006) Bardaskan Geology Map 1:100,000 No.7560, *Geological survey of Iran*.

Sneed M, Brandt JT (2015) Land subsidence in the San Joaquin Valley, California, USA, 2007–2014. *Proceedings of the International Association of Hydrological Sciences*: 372, 23-27.

Stocklin J, Nabavi MH (1973) Tectonic map of Iran, *Geological Survey of Iran*.

Taheri J, Shamanian GH (1998) Kashmar Geology Map 1:100,000 No.7660, *Geological survey of Iran*.

Üstün A, Tuşat E, Yalvaç S, Özkan İ, Eren Y, Özdemir A, Bildirici İÖ, Üstüntaş T, Kırtıloğlu OS, Mesutoğlu M, Doğanalp S (2015) Land subsidence in Konya Closed Basin and its spatio-temporal detection by GPS and DInSAR, *Environmental Earth Sciences* 73(10): 6691-703.

Yamamoto S (1995) Recent trend of land subsidence in Japan. *IAHS Publications-Series of Proceedings and Reports-Intern Assoc Hydrological Sciences* 234: 487.

Ward PJ, Marfai MA, Yulianto F, Hizbaron DR, Aerts JCJH (2011) Coastal inundation and damage exposure estimation: a case study for Jakarta. *Natural Hazards*: *6*(3), 899-916.

Wellman HW (1966) Active wrench faults of Iran, Afghanistan and Pakistan. Geologische Rundschau 55(3): 716-35